

Observation of complex functional cortical patterns in brain cognition

Jasleen Gund^{1,2} and R.K. Brojen Singh^{1*}

¹*School of Computational and Integrative Sciences,*

Jawaharlal Nehru University, New Delhi-110067, India.

²*Cognitive Brain Dynamics Lab, National Brain Research Centre, Manesar-122050, India.*

Synaptic plasticity and neuron cross-talk are some of the important key mechanisms underlying formation of dynamic clusters of active neurons. The essence of this study is to model and decipher the mechanism of emergence of a task-specific functional connectivity among a population of neurons. We have used our proposed neuron activity pattern (NAP) model to define an assorted range of interactions and simulated across a 2D lattice with two-state (firing/non-firing) neurons. We observed the emergence of scale-free, hierarchically organized ordered patterns of active neurons, that we call as functional cortical patterns (FCPs), only at the near-critical phase transition. We have done extensive topological characterization of FCPs and tested its congruency with the functional brain networks obtained from the empirical electrophysiological data of a visual stimulus task. Our results of network theory attributes, fractal analysis and functional cartography have confirmed the transitioning effect while generation of FCPs. This gives us strong implication that the functional neuronal system supports far-from-equilibrium dynamics upon receiving a stimulus. Our investigation for the long, critical and short-ranged interactions has lead to an interpretation that near-critical transition phase is a spectrum of critical temperatures (coupling strengths) being affected by the distance between the neurons. The range of interaction among neurons plays an important role in defining the functional severity of the neuronal circuitry. We propose that interaction range as a function of coupling strength drives connectivity in an augmenting fashion as we observed an increase in coupling strength from short to long-range interactions, among the population of neurons. This gives us insight towards the intensity of cognitive behaviour, which is attained by multiple stimulus attempts.

Keywords: Long-range Ising model, Neuron activity patterns, task-specific cognition, Brain functional networking, Near-critical dynamics.

I. INTRODUCTION

The phenomenon of global features of complex cognitive functions in the brain arise from the organization of basic functions systematically coordinated in localized brain regions [43]. These two aspects of brain organization are reflected in brain cortical functions and evolve continuously through internal and external perturbations. Hence, human cognition can be thought of as a water surface where patterns in the form of ripples dwell on its surface upon receiving perturbations from outside. The fluidity of consciousness is reflected through the highly dynamic behaviour of brain activity [16]. We can merely access those spatio-temporal patterns of brain activity through various electro-physiological and neuro-imaging techniques in order to understand the underlying dynamics. Electroencephalogram (EEG) is one such technique to measure electrical brain activity with high temporal resolution. The functional spatio-temporal clusters of neurons in the cortical layers of the brain is a consequence of various biological factors affecting the concentration of neurotransmitter, transfusion of ions through ion channels and voltage generated across the membrane of pre and post-synaptic neurons [40, 67]. These biological factors determine the strength of the diffused signal among neurons and neuronal organization. Such recurring signals strengthen the circuitry of the neuron cluster allowing it to learn and memorize a specific function in the brain and rewiring among these complex functional patterns lead to varied cognitive abilities of the brain [19, 24, 58, 61, 62]. But, how the synchronous neuronal activation and generation of functional patterns lead to the execution of a cognitive task is a riddle to solve. The basis of understanding the complex cognitive functions would begin through studying the network dynamics of the interacting local and global neurons. In shaping the functional network topology of the brain, the interaction range of the cortical functional regions in the brain and neurons within them plays a significant role. And it would be interesting to know how this range is determined for information processing and shaping neural circuitry among the neurons. The Ising model is a simple physical model that could explain the

*Electronic address: brojen@jnu.ac.in (Corresponding author)

ferromagnetic behaviour with domain coarsening of the two-spin lattice system through inter-molecular interactions imprinted by some range and concurrent computation of the Hamiltonian energy as a driving factor for the system evolution [45]. In our foregoing work, we proposed the *neuron activity pattern or NAP model* which is based on the kinetic Ising model system [33]. In that work, we established a critical interaction range that demarcates the long and short ranges of interaction. Our approach evaluates the role of various interaction ranges on the strength of coupling and the overall Hamiltonian dynamics, as compared to the Onsager result that solved for only nearest-neighbour interactions [51]. It has been shown in [33] that each interaction/coupling range has their unique critical temperature for generating spin clusters at the near-critical regime of phase transition though, their overall dynamical behaviour has followed universal scaling laws. Our anticipation led to the conjecture that cortical neurons might follow a second-order phase transition near-criticality to generate patterns of active neurons in response to a signal. However, the emergence of these functional clusters and their organization are still an open question. We have termed these patterns of neuronal activity as functional cortical patterns or FCPs.

In this study, we have generated model-based networks on the basis of, firstly, different ranges of interaction (long, critical and short) and secondly, another important parameter i.e. Temperature to define below, near and above criticality regimes. We have taken this architecture, further, to characterize temporal correlations based network connectivity of FCPs in our model data and found its congruency with the task-specific brain functional connectivity, attained through the empirical data. Since the functional connectivity reflects statistical dependencies between spatially distributed neuronal groups. We have made a comparison among networks of simulated and empirical data based on their topological characterization. This study has modelled the emergence of functional connectivity in the brain and to prove its fidelity we have applied different approaches such as network theory attributes, community detection, functional cartography of nodes and multi-fractal analysis. We have used the EEG data of a specific visual task on healthy human subjects for comparison with our model data [6]. We have addressed important features of functional cluster formation, their organization and properties at below, near and above criticality for each interaction range. The major concern of this work is, whether the FCPs generated through our neuron activity pattern model, could mimic the topological characteristics of task-specific functional brain connectivity.

II. RESULTS AND DISCUSSION

We first need to delineate the details of the model simulation in the next sub-section, succeeded by the deliberation over results.

A. Correlated neuron activity could optimize brain function

The concept of self-organization rightly defends the dynamics of complex systems [38] and also aids in understanding brain functionality [3]. Thinking of neural dynamics from a statistical mechanics window is a bit challenging but is ruling out since Ising model was used to explain the dynamical avalanches of neuron activity in the brain [16, 24]. In comparison with the Ising model a local neural network is not an equilibrium system as neurons constantly receives inputs from other neurons but the near-critical point of phase transition i.e. far from equilibrium could explain the dynamic equilibrium in complex systems. Also, the self-organizing dynamical systems expound that the brain works at a transition point when it receives the optimum signal strength [5]. Still, there is thirst for digging more into the complex dynamics of brain functionality. How brain does the transition towards a functional network that spans the cortical layers of brain, acquiring non-random synaptic connectivity for performing a cognitive task [57].

This research work has used the NAP model that was introduced in our previous work [33], therefore, the details regarding the Hamiltonian dynamics of the Ising model and its numerical simulation using the Monte Carlo Glauber kinetics with non-conserved magnetization has been briefly discussed here. The Ising model is one of the primitive models known to study phase ordering dynamics in a random distribution of spins under the influence of a critical parameter i.e. temperature (T). It had been used profoundly to explain the functional neuronal activity across functional brain networks [28, 30]. This makes us strongly presume that phase transition state is the critical state of brain functional dynamics at which cognitive actions take place. We have considered random allocation of two-spin configuration in a 2D-square lattice with periodic boundary condition in order to avoid the edge effect. We contemplated the cortical neuronal circuits coarse-grained into the firing and non-firing states of neurons (or group of neurons) represented by the two states of a spin s , $s = +1$ for firing and $s = -1$ for rest or non-firing neurons. The total energy of the system representing various internal fluctuations and diffusive processes in neurons that result in their activity and influences the activity of surrounding neurons is given by the following Hamiltonian to model long

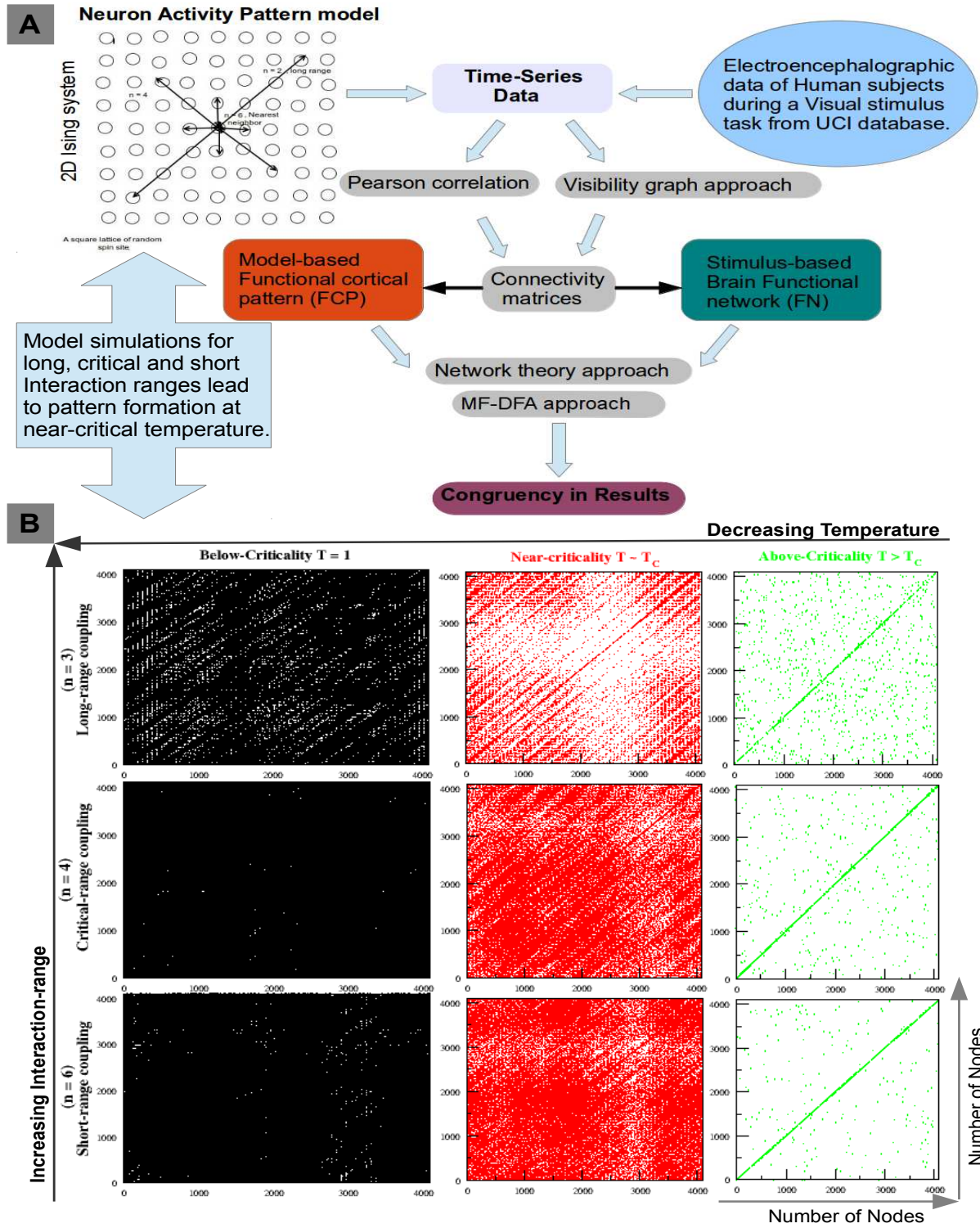


FIG. 1: The Recurrence plots of model-based functional cortical patterns (FCPs): **A**) Outline of the workflow used to characterize the model and empirical time-series data and to attain congruency in their functional activity patterns. **B**) For Long ($n = 3$), Critical ($n = 4$) and Short ($n = 6$) coupling ranges at synaptic strengths below-critical ($T = 1$), near-critical ($T \sim T_c$) and above-critical ($T > T_c$) strengths (as shown in black, red and green respectively), in a network of 4096 nodes. **Note:-** There is the formation of communities of active neurons at near-criticality for all the coupling range interactions.

as well as short-range interactions,

$$H = - \sum_{\langle ij \rangle} J(r_{ij}, n) s_i s_j, \quad s_i = \pm 1 \forall i, \quad (1)$$

Where s_i and s_j denotes the activity of neuron at site i and a neighbouring site j and J represents the coupling strength among neurons defined as a function of the distance between two i th and j th neurons given by, $r_{ij} = |r_i - r_j|$ which is confined by n , the coupling range in the system. Then one can model J by power-law behaviour given by, $J(r_{ij}, n) = \frac{J}{r_{ij}^n}$ [14], where, d is the dimension of the system, and n can be expressed as $n = d + \sigma = 2 + \sigma$ [8, 27] which can qualify for *short-range* for $\sigma > 2$, whereas for *long-range* for $0 < \sigma < 2$ [31, 55]. Further, $J > 0$ always (ferromagnetic case) and $n > 0$ [14]. We have taken a 2D square lattice of spins with side L and $N = L \times L$ being the total number of spin sites. To define coupling range we have assumed the centre of the 2D square as the reference origin to delimit the maximum distance for the spins to interact. The incircle of radius $r = L/2$ is the approximated area of the spin distribution which we have considered to calculate the potential energy, U , of the system. In order to capture the thermodynamical parameters of the system, one can define the following potential function $U(n)$ as a slowly decay potential function [14, 16], where $n = 2 + \sigma$ for the 2D system, scaling $J \rightarrow J/N$ in the limit $N \rightarrow \infty$ and using Euler-McLaurin sum formula [12], we get the potential energy function for each interaction range n as follows, [33]

$$\begin{aligned} U(n) &= \lim_{N \rightarrow \infty} \frac{1}{N} \sum_{\langle i, j \rangle} \frac{J}{r_{ij}^n} \approx \lim_{N \rightarrow \infty} J \int_1^{\sqrt{N}} dr g(r) r^{3-n} \\ &= \lim_{N \rightarrow \infty} J \begin{cases} \frac{1}{2} \ln(N), & \text{for } n = 4 \text{ (critical)} \\ \frac{1}{n-4} (1 - N^{2-n/2}), & \text{for } n > 4 \text{ (short range)} \\ \frac{1}{4-n} N^{2-n/2} & \text{for } 0 < n < 4 \text{ (long range)} \end{cases} \end{aligned} \quad (2)$$

where, $g(r)$ is the pair distribution function such that $g(r) \rightarrow 1$ for $r \gg 1$. Critical parameters of the 2D system can be calculated from the force derived from the potential in equation (2), at the critical point where singularity arises in the solution of the system [35]. Following this technique one can estimate critical temperature from the numerically derived closed form approximated equation [35] given below,

$$\frac{U(n)}{k_B T_c} = 1 + \frac{f_2}{U(n)^2} + O(U^{-4}) \quad (3)$$

where, $f_2 = \sum_{\langle i, j \rangle} J(r_{ij}, n)^2$, which can be calculated for the 2D system by following the procedure mentioned above i.e. scaling $J \rightarrow J/N$ in the limit $N \rightarrow \infty$. Now using Euler-McLaurin sum formula [12], f_2 is given by,

$$\begin{aligned} f_2 &= \lim_{N \rightarrow \infty} \frac{1}{N} \sum_{\langle i, j \rangle} \left[\frac{J}{r_{ij}^n} \right]^2 \approx \lim_{N \rightarrow \infty} J^2 \int_1^{\sqrt{N}} dr g(r) r^{5-2n} \\ &= \lim_{N \rightarrow \infty} \frac{J^2}{2} \begin{cases} \left[1 - \frac{1}{N} \right], & \text{for } n = 4 \text{ (critical)} \\ \frac{1 - N^{3-n}}{n-3}, & \text{for } n > 4 \text{ (short range)} \\ \frac{N^{3-n} - 1}{3-n} & \text{for } 0 < n < 4 \text{ (long range)} \end{cases} \end{aligned} \quad (4)$$

Now using equations (3), (2) and (4) we could able to arrive at an expression for finite critical temperature given below,

$$\begin{aligned} T_c(n, N) &= \frac{1}{k_B} \frac{1}{1 + \frac{f_2}{U(n)^2}} \\ &= \frac{J}{k_B} \begin{cases} \lim_{N \rightarrow \infty} \frac{N [\ln(N)]^3}{2N + N [\ln(N)]^2 - 1}, & \text{for } n = 4 \text{ (Critical)} \\ \frac{4(n-3)}{(n-2)^2(n-4)}, & \text{for } n > 4 \text{ (short range)} \\ \lim_{N \rightarrow \infty} \frac{2}{4-n} \frac{N^{3(4-n)/2}}{2N^{4-n} + (4-n)^2 \left[\frac{N^{3-n} - 1}{3-n} \right]} & \text{for } 0 < n < 4 \text{ (long range)} \end{cases} \end{aligned} \quad (5)$$

From the above equations (5), we could able to understand that for fixed systems size N both short-range and long-range interaction of neurons contributed to J lowers in T_c allowing to work the neurons at a modified phase. On the other hand, for fixed n , T_c increases as N increases both in critical and long-range regime. The

quantities such as range of interaction n (or coupling range) and coupling strength J controls the order parameter i.e. temperature T of a spin-lattice system. However, there are debates on the estimation of T_c dependence on J in 2D system. Even though the relation between T_c and J was obtained analytically in 2D system as $\sinh(2J/k_B T_c) \approx 1$ [51], numerically calculated $J/k_B T_c$ using Monte carlo techniques in such systems within finite size scaling formalism was found to be varying in the range $J/k_B T_c \rightarrow [2.269 - 2.29]$ [7]. The reason for variation in the critical parameter value could be due to finite size (N) of the system [7], and T_c depends on size N except for short-range interaction ($n > 4$). The critical temperature T_c can be defined in terms of J/k_B , however, through our model simulations of random spin lattices, we have got the float values of T_c for various long and short interaction ranges (see Fig.1 of ref. [33]), signified by the sudden drop in the total magnetization (order parameter) of the system.

Our idea states that this modelling framework mimics the underlying dynamics among a population of neurons. This study intends to relate the terminology being used in two different yet relatable systems, to characterize the brain as a dynamic physical system. We have defined the temperature, analogously, as the global synaptic strength given to a system of neurons (or groups of neurons) that generates the synchronous simultaneous activation of neurons sharing common synaptic strength. Therefore, the critical temperature would mirror the optimal perturbation (stimulus) imparted to the system i.e. relayed and associated in the form of synaptic strength in the brain. We have taken a 2D 64×64 lattice system of 4096 spin sites depicting either firing or non-firing neuron state, allocated randomly, and simulated for 500 monte carlo steps at a defined global synaptic strength. Our approach examines the inter-neuronal connections for long, short and critical coupling ranges at different *global* synaptic strengths (T) as categorized into three stages, below criticality, near-criticality and above criticality. The below criticality is defined as the temperature below the phase transition temperature but above the mean-field temperature i.e. $0 < T < T_c$. We have considered $T = 1 \frac{J}{k_B}$ as below critical temperature for all coupling ranges. However, the near-critical transition temperature, T_c , is different for the long ($T_c \sim 2.9 \frac{J}{k_B}$), critical ($T_c \sim 1.9 \frac{J}{k_B}$) and short ($T_c \sim 1.4 \frac{J}{k_B}$) ranged interactions, based on their respective dynamics (see Fig.1 of ref. [33]). The spin-flip kinetics within Glauber kinetics algorithm defines the spin acceptance probability and also assumes ergodicity, however, the spin is chosen randomly [7, 48]. The system quenches from a random disordered to ordered lattice phase and lead to the formation of domains/patterns of functional activity [61]. The Monte Carlo simulations for a particular coupling range n and global synaptic strength T has generated the temporal activity data based on the state of each neuron. In order to substantiate the global system *behaviour*, we did average over temporal data of 10 ensemble sets in each case. The averaged time-series data is further used to construct binary undirected graphs by defining inter-neuronal connections using the Pearson correlation coefficient for different coupling range and strengths (see Methods). Thus, our analysis of a 2D lattice of neurons with fixed position and randomly allocated activity at each site lead to the emergence of FCPs of synchronous activity at the near-critical temperature, the optimum synaptic strength.

B. Model-based functional cortical patterns

The neuron activity patterns can be imprinted in a connectivity matrix based on the correlation in the activity of neurons. The temporal correlations of the neural activity has been translated in the form of binary connectivity matrices. We have applied different approaches for building the connection matrix out of the model and empirical time-series data as mentioned in the work flow-chart as shown in Fig.1A. We have tagged the model-based functional clusters of synchronous activity as FCPs. On the other hand, the visual task-based EEG time-series has been transformed into a functional brain network, FN, using the visibility graph approach [41]. We have acquired significant congruence in the FCPs and FNs in their topological properties and functional characterization by applying the network theory and multi-fractal approaches [37, 58]. The model simulations at various interaction ranges and temperature strengths substantiate the emergence of functional patterns of activity only at the near-critical strength as depicted through the recurrence plots in Fig.1B. In this work, we have extended the interpretation of our model data and applied a fixed global synaptic strength which determines the intensity of overall coupling among the system of N neurons, being classified as below-criticality, near-criticality and above-criticality of the phase transition dynamics. The critical temperature T_c , which signifies the state of near-critical phase transition, is found to mimic with the optimum synaptic strength to coordinate short and long-range neurons in the brain for the generation of functional clusters of neurons at local and global levels.

The emergence of FCPs in our model is the result of self-organized criticality that formulates the functional pattern of neurons in the brain [39]. These FCPs could mimic the functional networking that emerges in the brain cortex with task-specific activation of neurons. The recurrence plots in Fig.1B shows the emergence of FCPs being more prominent at near-critical temperature, T_c for each coupling range. The long-ranged coupling at $T = 1$, is showing

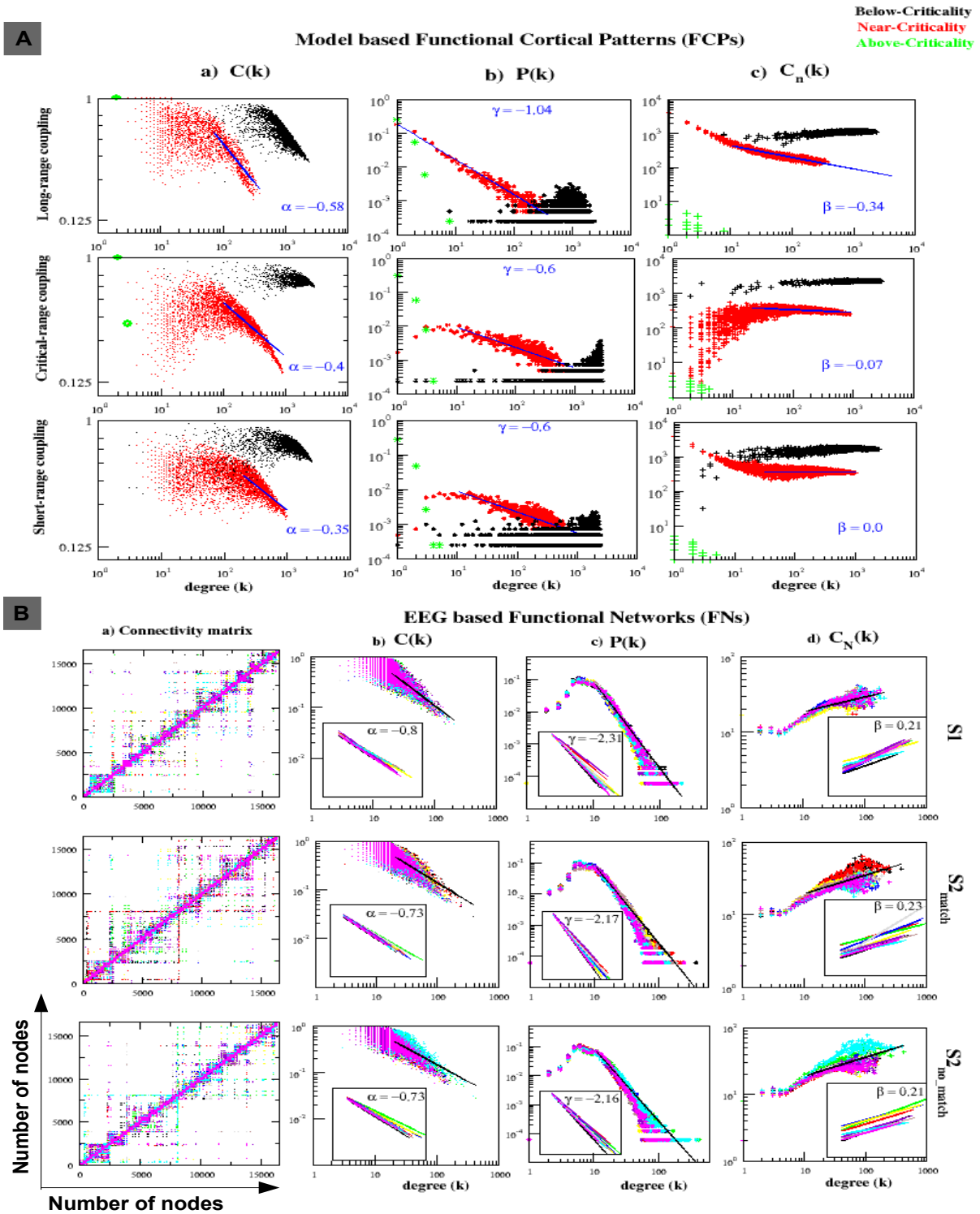


FIG. 2: Basic network attributes of model-based FCPs and EEG-based FNs: **A)** FCPs for the three distinguished coupling ranges at synaptic strengths below criticality (in black), near-criticality (in red) and above criticality (in green). The columns exhibit a) clustering coefficient, $C(k)$, versus degree (k) plots with degree exponent α . b) The probability of degree distribution, $P(k)$, plots with degree exponent γ c) The Neighborhood connectivity, $C_n(k)$, plots with degree exponent β . **B)** a) The connectivity trend of EEG data based FNs generated for three visual stimulus conditions S1 (single image shown), S2_match (two similar images) and S2_nomatch (two dissimilar images) of one subject with 10 trials shown in different colours in each case. The columns b), c) and d) illustrates the $C(k)$, $P(k)$ and $C_n(k)$ plots versus degree (k), respectively. The insider plots depict power-law fitting trend of 10 subjects with their average degree exponents. **Note** - In all the coupling ranges long, critical and short their is transition shift at near-criticality (shown in red) for all the three basic network attributes that characterize the hierarchical and scale-free organization through the power-law behaviour of their heavy-tailed distributions. The network measures are subsequently in similar trend for near-critical FCPs and EEG based FNs, apart from the obvious disparity among subjects.

very less clustering and therefore it has many random connections not forming any ordered patterns or domains as reflected in recurrence plots. However, at near-critical synaptic strength ($T \sim T_c$), the transition to critical phase allows the formation of a number of functional patterns or domains. We could signify the near-critical transition as a state of attaining the optimal synaptic strength to construct synchronous functional patterns of neural activity and that could mimic the conscious state of a simple cognitive task in the brain [24]. Further, at above-criticality ($T > T_c$) these patterns are violated due to enormous decline in the randomness of neuronal connections, causing break-down of neuronal self-organization. Also, the high synaptic strength could signify the abnormal state with loss of functional connectivity as observed in diseases such as Alzheimer's etc [63]. The similar trend is followed by the critical and short coupling range (see in Fig.1B). However, the underlying dynamics is different for short and long-range interactions. The long-range coupling ($n = 3$) has been speculated with fast dynamical clustering at near-critical temperature, $T_c = 2.9 \frac{J}{k_B}$ whereas, short-range coupling ($n = 6$) has exhibited slow dynamics at $T_c = 1.5 \frac{J}{k_B}$ [33]. From equation (5), short-range T_c ($n = 6$) is given by $T_c = \frac{3}{8} \frac{J}{k_B}$. Whereas, since $\lim_{n \rightarrow 3} \frac{N^{3-n}-1}{3-n} = \lim_{n \rightarrow 3} \frac{-(\ln(N))N^{3-n}}{-1} = \ln(N)$, the long-range T_c ($n = 3$) is given by,

$$T_c(N) \approx \frac{J}{k_B} \frac{2N^{3/2}}{2N + \ln(N)} \quad (6)$$

This shows $T_c(N)$ depends on system size, N , for long-range coupling only. These changes in T_c could suggest the enlargement of FCPs, generated with respect to short and long-range depending on N , with increasing synaptic strength signifying the local and global coupling over population of neurons [23, 39].

C. Network topology and characterization.

The complex network theory approach, originated from graph theory, delineates the consanguineous activity of neurons in terms of quantitative measures [13, 52]. We have applied the network theory attributes here to characterize the functional networks generated through the neuro-physiological EEG data set and the simulated FCPs of the population of neurons.

1. Properties of model-based FCPs:

We have computed network theory attributes to study the topological properties of the FCPs generated (as shown in Fig.1), using our model approach. The network attributes calculated here, represents the topological information of the connected undirected networks generated for different coupling ranges of interaction. The sheer transition in the clustering coefficient distribution, $C(k)$, plots from below (black) to near-critical state (red) (Fig. 2A column a) apparently classifies the organization of a functional cluster in a hierarchical pattern as exhibited through the power-law scaling behaviour $C(k) \sim k^{-\alpha}$ as a function of degree k with scaling exponent α for all the distinguished coupling ranges (long, critical and short). The data has been plotted on a logarithmic scale with non-linear curve fitting to expose the power-law scaling behaviour. The cases with an initial scattering of data points have shown that the power-law is exhibited only by their long heavy tail whereas, other cases have shown power-law scaling constituting whole or majority of data points. The power-law distribution has been confirmed by the algorithm given by Clauset et al. [17]. However, at the above critical state (green) due to increased in the randomness of neuronal firing there are very fewer connections to form a functional pattern. Since α for long-range coupling provides larger value ($\alpha = 0.58$) as compared to short-range coupling ($\alpha = 0.35$), the long-range coupling at near-critical temperature probably enhances the active self-organization of neurons and local effects are allowed to participate in global phenomena. The probability of degree distribution, $P(k)$ again exhibits well defined fractal nature $P(k) \sim k^{-\gamma}$ at near-critical temperature with larger value of scaling parameter, $\gamma = 1.04$, for long-range coupling and shows similar transition into a power-law function, thus, substantiate the presence of high degree nodes having less occurrence probability in the neural network. Similarly, the neighbourhood connectivity distribution also follows power-law nature, $C_n(k) \sim k^\beta$ with k , and near-critical temperature exhibits positive β value for short-range and critical couplings indicating possibility of formation of rich-club, where some of the hubs hand in hand together to control the network. However, long-range coupling try to initiate neurons against this rich club formation (negative value in β). This assures that long-range coupling tries to keep hierarchical organization in the functional cortical pattern near-critical temperature phase. However, short and near-critical range couplings try to bring the network towards near scale-free features, where $C_n(k)$ becomes nearly independent of k and β becomes positive indicating significant importance of a group of hubs (rich club formation) respectively. Further, the behaviour at below critical temperature

exhibits positive β values (black colour data) for all types of coupling ranges (short, critical and long) which is a clear indication of rich club formation showing the significantly important role of hub groups in regulating FCPs. On the other hand, in the case of the above criticality regime, proper and clear behaviour of network properties in the FCPs are not exhibited for all coupling ranges.

2. Properties of EEG based functional networks:

The EEG time-series data of the whole brain while visualizing a particular single object (S1), two matching objects (S2 match) and two different objects (S2 nomatch) in human subjects has been taken from the UCI database. Since the networks or visibility graphs constructed from the EEG time-series data carry the properties embedded in the EEG data [41], characterization of these networks of various subjects may highlight how these brain functional networks work and organize themselves. Each node in the constructed networks corresponds to the time step mapped to the EEG time-series data which could be the resultant of the algebraic sum of all possible interacting neuronal signals (including all possible coupling ranges) at that time step. Hence, these nodes in the networks could be thought of as the representations of the interacting neurons at various cortical regions of the brain at various time steps collected by the EEG probes as signals. Further, these functional networks (FNs) thus constructed from the EEG data of the subjects, while doing a visual task, exhibit well-defined clusters of represented neurons with slight variation in their sizes and properties due to the different paradigms (S1, S2 match and S2 nomatch) (Fig. 2B column a). These FNs of the subjects shown to specific visual stimulus task declares the dynamics of the neuronal functional patterns specific to the visual cortex.

Now the connectivity plots and topological characterization of the EEG-based FNs show clear emergence of clusters/modules/domains of varied sizes in all subject cases (S1, S2 match and S2 nomatch) (Fig.2B a). Similar to our theoretically obtained results (in Fig. 1), the behaviour of the topological properties of these networks (we presented the results only for 10 trials of a single subject and its also true for all trials of the subjects we have taken from the UCI database for analysis) follow power-law nature indicating the fractal nature of the system. More specifically, the properties of our neuron activity pattern model near-critical temperature is closely similar to the properties of FNs constructed from EEG data. Then, these topological parameters can be represented by,

$$\Gamma(\mathbf{k}) \sim \mathbf{k}^{\mathbf{F}}; \quad \Gamma(\mathbf{k}) = \begin{bmatrix} P(k) \\ C(k) \\ C_n(k) \end{bmatrix}, \quad \mathbf{F} = \begin{bmatrix} \gamma \\ \alpha \\ \beta \end{bmatrix} \rightarrow \begin{bmatrix} -2.16 - 2.31 \\ -0.73 - 0.8 \\ 0.21 - 0.23 \end{bmatrix} \quad (7)$$

The positive value in exponent β in C_n indicates the assortativity property in the network (Methods) which enable significant hubs in the network to coordinate among them [20]. Further, the emerged modules/clusters follow hierarchical features and hence have a significant correlation among them (Methods). Because of these two reasons these FNs most likely exhibit *rich-club* formation which is consistent with the experimental report on the brain [65]. This means that the rich-club formation of significant hubs in the hierarchically self-organized neuronal system may probably act to stabilize the system both at local and global levels.

Our interpretation theory professes as if a slow and weak signal (say at $T < T_c$) propagates among the cluster of neurons creating a pre-conscious state for neurons and then a perturbation (signal) would provide an optimal synaptic strength (T_c) that could drive the system towards a functional cognitive state. (This could give sense to the condition when there are many processes or thoughts that passes through our mind in an unconscious state and an external stimulus is required to attain the conscious state.) The $C(k)$ and $P(k)$ distributions have been found to be in accordance with the brain functional connectivity network attributes based on the experimental data as reported in [24, 60]. The results shown in [24] reflects the functional network attributes while listening to music and finger tapping. The complexity in functional brain networks has been classified as scale-free considering spatio-temporal neural activity through neuro-electrical and imaging techniques [4]. From this, we could affirm the validity of our model approach in characterization of the emerging FCPs formed in the brain while some specific cognitive task is done[66]. Thus, the network representations of nodes at $T \simeq T_c$ for long, critical and short-range interactions assures the self-organization of nodes into an FCP which exhibits scale-invariant and hierarchical organization. This supports our understanding that the self-organization of the interacting neurons is maintained with the emergence of FCPs for disparate ranges at near-criticality [23].

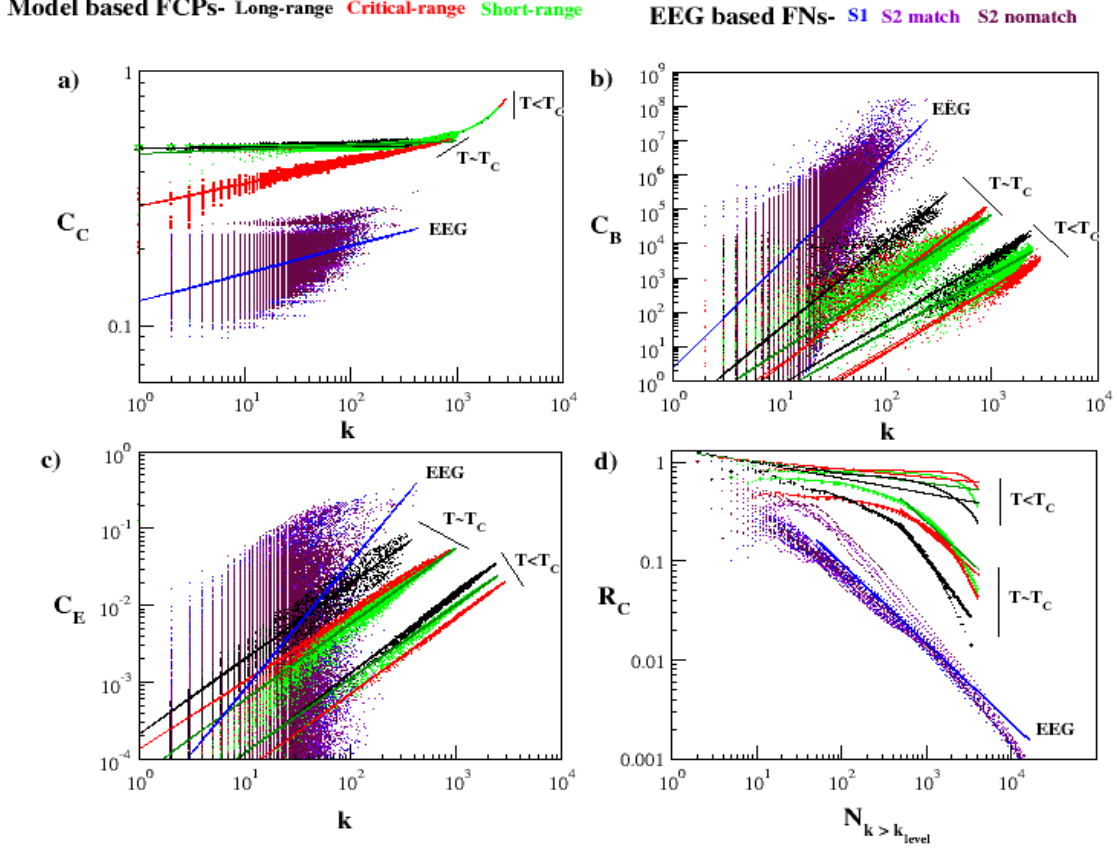


FIG. 3: **Comparative analysis of network attributes:** The model-based FCPs have been analysed to mark the near-critical phase transition in comparison with the EEG data based FNs. a) The closeness centrality, $C_C(k)$, versus degree (k) plot with degree exponent δ . b) The betweenness centrality, $C_B(k)$, plot with degree exponent λ . (C) The eigen-vector centrality, $C_E(k)$, plot with degree exponent ϵ . (D) The rich-club coefficient, $R_C(k)$, is plotted against $N_{k > k_{level}}$ i.e. number of nodes with degree (k) greater than particular k_{level} . **Note-** The near-critical FCPs have shown the right transition shift towards the FNs of a visual task-based data. For a particular degree node the C_B and C_E value has increased to make its role more economical, though not much change in C_C values observed. The $R_C(k)$ plot has shown power-law trend with heavy tail distribution.

D. Centrality and rich-club measures: hierarchical to scale-free transition

The roles and characterization of the significant hubs in the brain networks, in which emerged modules and sparsely distributed hubs work in a self-organized manner, can be well studied and compare using centrality measurements and rich-club analysis of the networks constructed from both neuron pattern activity model and EEG data. The centrality measures, as shown in Fig.3, characterizes the FCPs, at below and near-criticality for all coupling ranges and does a fair comparison with the FNs generated through the EEG data of a visual stimulus. Since the closeness centrality measurement C_C of a node is estimated by the inverse of average distances of the node with the rest of the other remaining nodes [42], a large value of C_C , which is quantified by small average path distance, provides significant importance of the node in regulating the network. The C_C as a function of k follows power-law nature, $C_C(k) \sim k^\delta$, both in proposed model network and network constructed from EEG data except the value C_C in networks of EEG data is comparatively smaller than that of the model network (Fig. 3 (a)). The behaviour of C_C for model network at near-critical temperature, $T \sim T_c$ for critical interaction range is closely similar to that of the network from EEG data, where, C_C increases with k indicating a significant role of high degree hubs in regulating brain network in terms of fast information processing of the neurons may be by coordinating the high degree nodes in all the modules of the networks. On the other hand, short and long-range correlation of the neurons again trigger more importance of the hubs moving towards the scale-free phase where hubs are more important than modules in controlling the networks. For higher degree nodes, the value is less at $T \simeq T_c$, this confirms the rareness of hubs in the network.

Betweenness centrality of the networks, which is another centrality measure from the number of paths passing through each node from the rest of the nodes in the network, quantify the volume of traffic diffusing through each node in these networks [11, 42], and found that it follows power-law behaviour, $C_B \sim k^\lambda$ in both model and EEG data networks (Fig. 3 (b)). Since C_B increases as k increases, it indicates that high degree nodes have high traffic of information, and they play a crucial role to control and stabilize the network. In this case, the behaviour of the C_B for all neuron coupling regimes (short, critical and long-range) are closely mimic with that of networks of EEG data in qualitative sense (indicated by nearly parallel fitting lines on the data points). This nature of $C_B(k)$, characterizes the cluster at $T \simeq T_c$ with higher value for high degree nodes and thus ensures greater significance of those nodes in fast information transmission across the network [13]. Similarly, the properties of the eigen-vector centrality, which is the measure of influence of a node to any other nodes in the network that could induce long-term traffic risk [10], show power-law nature, $C_E(k) \sim k^\epsilon$ to both for model and EEG data based networks indicating closely mimic behaviour (due to nearly parallel fitted lines). This eigenvector centrality, $C_E(k)$, further depicts the intensity of most prominent nodes in networks and found that network is highly communicative at $T \simeq T_c$ with low cost. Hence, high degree nodes have significant influencing capability to other nodes as well as more risk of attack to them. These high degree nodes could be generally target nodes of any brain disorder (disease, functional disorder etc).

Now the behaviour of all three centrality measurements (C_C, C_B, C_E) indicates the significantly important roles of high degree nodes in both model and EEG data based networks in terms of fast signal processing, regulation of information traffic, influencing other nodes in the network. This could be a clear signature of rich-club formation in these networks, indicating the significant role of the high degree hubs in regulating the networks but removal of these hubs will not cause network breakdown. Another thing depicts through our results are the presence of high degree nodes in long as well as short-range connections. This is in accordance with the experimental results done by [50], where they found high degree neurons through direct recording from up to 500 neurons in slice cultures of mouse somatosensory cortex. In all centrality measurements of model based FCPs at $T \sim T_c$ and $T < T_c$, long-range neuronal coupling contribution is higher than the remaining critical and short-range interactions indicating a significantly more important role of long-range interaction of neurons in FCPs. One possible reason for more importance of long-range neuronal interaction in FCPs could be enhanced propagation of localized properties/perturbation, driven by short-range neuronal interaction, at the global level for better cross-talk to keep network stabilization in a self-organized manner.

The plot in Fig. 3d, quantifies the rich-club coefficient, R_C , as a function of $N_{k > k_{level}}$, which is the number of nodes with degree (k) greater than a particular k_{level} , where $k_{level} = 1, \dots, \max(k)$ (see Methods). This has encountered presence of hubs (high degree nodes) connecting module/communities patterned in a rich-club arrangement, to maximize communication at low-cost maintaining robustness of the network. The comparative analysis has shown that FCPs at below critical strength are far from the behaviour of the empirical data networks used here. However, at near-critical strength, FCPs leads to a shift towards the behaviour of FNs generated. The degree exponents of various network attributes calculated have been shown in Table-1 for all coupling range and strengths along with the EEG data. Apart from the visible differences in degree exponents of our model and EEG clusters, the trend followed by them in network attributes are quite similar.

E. Modular organization: Is near-critical state active

Modularity signifies the formation of community or modular structure in the network [49]. The network centrality measures characterize the important nodes that determine the functional efficiency of the network. However, defining the role of a node based on its position within the module and participation among inter-linking modules is an effective way to portray complex networks [32]. In Fig.4A (a), we compare the community affiliated structure, (C_i), of long, critical and short-ranged coupling networks with the FNs of the EEG data. In column Fig. 4A (b), the within-module degree, Z_i , versus participation coefficient (P_i) plots relate the organization of influential nodes based on their intra- and inter-module links. The results show that the near-critical FCPs has marked good coherence with the EEG data. In Fig.4B, based on the categorization of nodes done in [32], we have shown the transition in role and position of module nodes in the near-critical modular networks. The P_i versus degree k plots for the distinguished coupling ranges at below-critical and near-critical synaptic strengths has been shown in columns Fig. 4B (a) and (b) respectively. The nodes have been labelled as module hubs and non-hubs with $Z_i \geq 2.5$ and $Z_i < 2.5$ respectively. The further segregation depending on their P_i values describes nodes as, $R1$ ultra-peripheral non-hubs ($P_i \leq 0.05$) with all the edge connections in the same module; $R2$ peripheral non-hubs ($0.05 < P_i \leq 0.62$) with mostly intra-modular edges; $R3$ connector non-hubs ($0.62 < P_i \leq 0.80$) with many inter-modular edges; $R4$ kinless non-hubs

($P_i > 0.80$) with homogeneous sharing of connections among modules; $R5$ provincial hubs ($P_i \leq 0.30$) with most of the intra-modular connections; $R6$ connector hubs ($0.30 < P_i \leq 0.75$) with majority of inter-modular associations and $R7$ kinless hubs ($P_i > 0.75$) with homogeneous associations among all the modules [32]. In our results of Fig.4B, the transition of temperature from below to near-critical regime leads to the occurrence of non-hub connector nodes, $R3$, (shown in green) in all coupling ranges. The early emergence of such hub nodes in long-range coupling could be due to its fast neuronal dynamics. Also, the near-critical FCPs has shown transition to the optimum hierarchical organization of connector hub nodes, $R6$, and peripheral non-hub nodes, $R2$, with respect to the degree for all coupling ranges, validating its functional modularity. The FNs of the EEG data (shown in violet), being a complex functional brain network, matches favourably with our model FCPs at the near-criticality regime. Further in Fig. 5, we have analyzed the probability of the degree distribution of nodes under a particular community, as constructed through the community affiliation Louvain method [9]. The modules generated through networks of below and near-critical FCPs has been shown in Fig. 5 (a) and (b), in respective different color for each module. For comparative analysis, the communities underlying the EEG data based networks have been shown in column (c) with quite a similar trend among various trials (shown in respective different colors) of a single subject. The below to near-critical transition signifies an increase in the number of communities. Also, the near-critical communities at short-range organize themselves towards small-world and tend to become hierarchical and scale-free at long-range as depicted through their degree distributions. This could be a signature to differentiate local and global coupling mechanisms in the functional brain networks which sounds helpful to tackle specificity of brain disorders.

F. Multi-fractal signature due to complex brain organization

Fractal characterization of a complex temporal signal has been done using the multi-fractal detrended fluctuation analysis (MFDFA) [37, 57]. The power-law scaling behaviour exhibited by the networks at near-critical strength characterizes the approximately self-similar temporal pattern formation, which further announces the existence of a fractal dimension to describe the complex organization and role of short and long-range correlation of the components of the system. The comprehensive methodology on *MFDFA* in [36, 57] signifies the presence of multi-fractality in biological complex systems reflected in time-series data analysis of the system. We have studied the presence of multi-fractality in self-organizing FCPs at below and near-critical strengths and compared the same with the EEG data generated FNs. In Fig.6 plot(a), the overall root mean square fluctuation function, F_q , for q in range -5 to +5 is showing variation of fast and slow evolving fluctuations over segments of scale s in the time-series, for each coupling range (long, short and critical) at $T < T_c$ and $T \simeq T_c$ and the EEG data as shown in respective colors. The scale of range 16 to 1024 has been used to calculate the function F_q at each scale s and is same for both the model and empirical EEG data. The slope of this scaling function F_q determines the q -order Hurst exponent H_q . The H_q is an important parameter to characterize multi-fractality as it captures the scaling behavior of small and large fluctuations in the time-series data, thus, its dependence on q validates the multi-fractal nature. In Fig.6(b), the negative q exhibits the scaling trend of small fluctuations and positive q represents the scaling behaviour of large fluctuations in the data segments of a particular scale. The Fig6(b) has shown variation mainly in the scaling nature of small fluctuations at negative q 's and depicts an almost similar trend for large fluctuations at positive q 's. The case of EEG data demonstrates the result of one subject each of $S1$, $S2_{match}$ and $S2_{nomatch}$ whereas the model data is the averaged result of 10 trials of time-series for all the three cases (long, short and critical). The H_q of small and large fluctuations in the model data might get affected because of the averaging of data. However, we are more concerned about the scaling trend of the near-critical transition results being similar with the EEG data rather than the below criticality. The Fig6(c) represents the q -order mass exponent t_q versus q , which exhibits the variation in mass exponent t_q with respect to large (+ve q) and small (-ve q) fluctuations. The Fig6(d), partitioned into two subplots, further represents the generalized fractal dimension D_q versus singularity exponent h_q for below-criticality in the left subplot and near-criticality and EEG data in the right subplot. The mass exponent t_q , is a factor used to define the fractal dimension. In Fig6(d), the clear transition in the h_q and D_q , from below to near-critical state, exhibits presence of multiple scaling exponents represented by the arc of the multi-fractal spectrum of long, critical and short coupling ranges that signifies an increase in complexity. The near-critical multi-fractal spectrum curves have shown high congruence with spectrum curves of the FNs of a visual task-based EEG data.

III. CONCLUSION

We have made an attempt to characterize cortical neuronal circuitry that emerges out in the brain during any cognitive assignment. In our model, the two-state dynamics has shown ordered pattern dynamics with the emergence of functional clusters, when it evolves at near-critical regime for all the interaction ranges. The emergent network

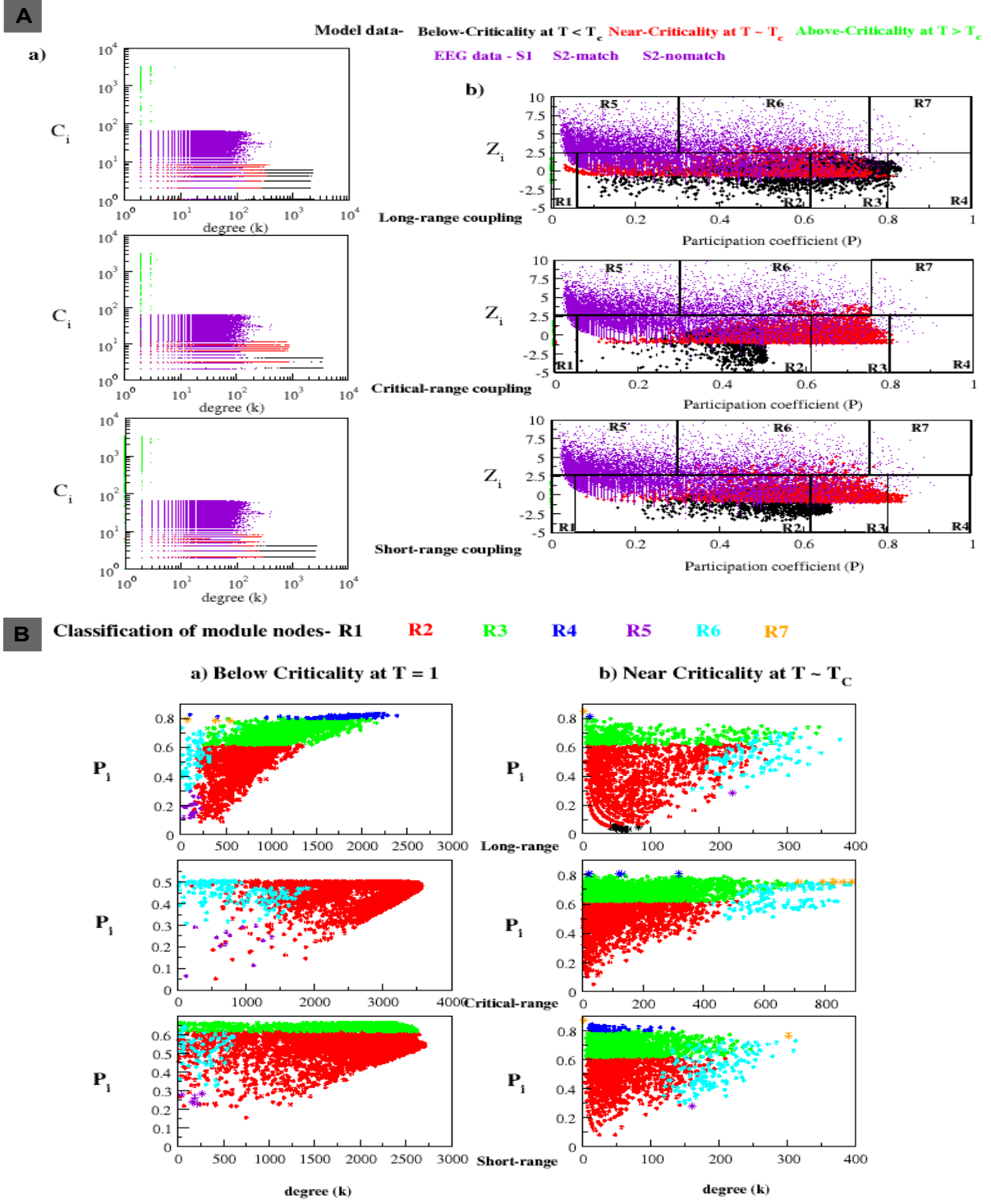


FIG. 4: **Community structure in networks of the model and EEG data:** **A)** The model-based FCPs for the long, critical and short-ranged coupling has been compared with the EEG data based FNs (shown in violet). **a)** The community affiliation index, (C_i), versus degree (k) plots. **b)** The within-module degree, Z_i , versus participation coefficient, P_i , plots exhibits presence of module-hubs based on the classification scheme defined as R1- ultra peripheral non-hubs, R2- peripheral non-hubs, R3- connector non-hubs, R4- kinless non-hubs, R5- provincial hubs, R6- connector hubs, R7- kinless hubs. **B)** The classification of module nodes, based on the Z_i and P_i values, and their organization depicted through the P_i versus degree (k) plots in the model generated FCPs for **a)** Below critical synaptic strength at $T = 1.0$ and **b)** Near critical strength of their respective T_c . The presence of various hub and non-hub nodes has been coded in respective colors shown in the figure. **Note-** The congruency of the EEG data (shown in violet) with the near-critical dynamics (shown in red) claims the model robustness. There is emergence of R3 non-hub connector nodes and R7 kinless hubs in the near- critical FCPs. Also, the organization of R2 peripheral non-hub nodes and R6 connector hub nodes is showing the right hierarchy with respect to degree upon transition to near criticality.

Degree-distribution of modules underlying each network

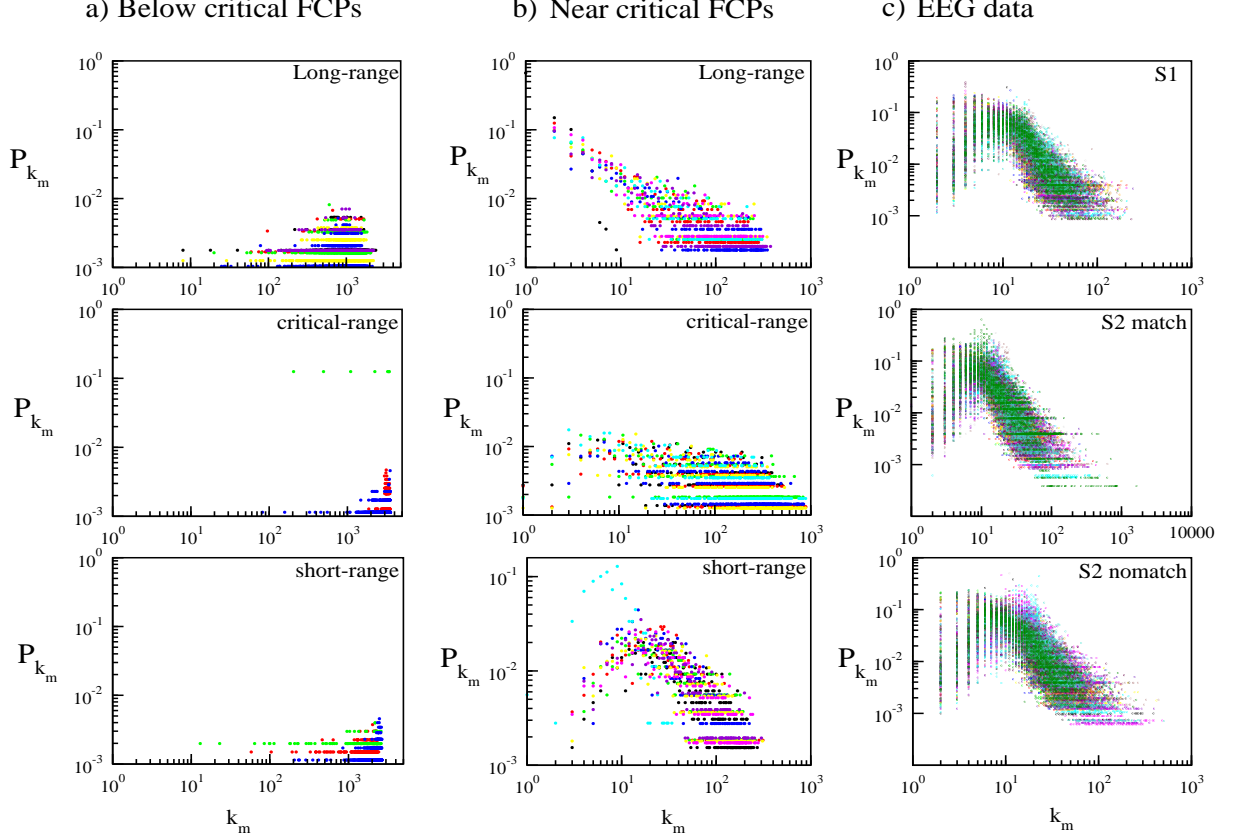


FIG. 5: **Analysis of Probability of degree-distributions in modules of networks:** In a) and b) columns for long, critical and short-range coupling we have shown probability of degree distribution, P_{k_m} , of each node degree k in module m of the below and near-critical FCPs, respectively. Here, different colors represent different communities. c) The column shows P_{k_m} versus k_m plots of the communities underlying the EEG data based networks for the three paradigms S1, S2 match and S2 nomatch. Here, different colors represent communities of various trials of a single subject. Note- The modules of near-critical FCPs at short-range follows poisson distribution that transitions to the scale-free organization at long-range coupling.

connectivity at near-critical strength, that we call as FCPs, symbolizes the emergence of functional connectivity in the brain. We have done extensive topological characterization of the FCPs and compared with the task-specific functional brain network of human subjects. In this comprehensive work, we have validated our insights of brain functionality by characterizing properties of self-organized functional connectivity embedded in the time-series data of task-specific activity. We have analyzed combined effect of both coupling strength and coupling range as drivers defining the interactions in our model. Through graph theory measures, the effect of coupling range on the network of neural population depicts clear transition in the dynamic state of connectivity at the near-critical strength ($T \simeq T_c$). This illustrates the transition from a randomly connected network to a hierarchical network that owns scale-free characteristics with the presence of hubs as shown by the heavy tail distribution of degree distribution plots. The probability of degree distribution $P(k)$ and clustering coefficient $C(k)$ plots, clearly, explains the emergent complex dynamics of FCPs. The dynamics of the networks at $T \simeq T_c$ for long, critical and short-range coupling is found congruent with the emergent functional connectivity in the brain while performing a specific cognitive task. The self-organization in the brain lead to the emergence of FCPs in the form of hierarchically organized functional modules as reflected from the power-law nature of the rich-club organization and centrality measures of the networks constructed [46, 66]. The presence of network centrality and rich-club behaviour, in similar trend with the EEG-based FNs, ensures the presence of coordinating hubs or dense modular cluster of neurons for effective communication in the model-based FCPs. This makes the functional pattern of neurons robust enough to maintain connectivity while wiring/rewiring among neurons as the dynamic pattern of connectivity among neurons affects the cost of information transmission [22]. The near-critical FCPs have shown the presence of $R6$, connector hubs, and

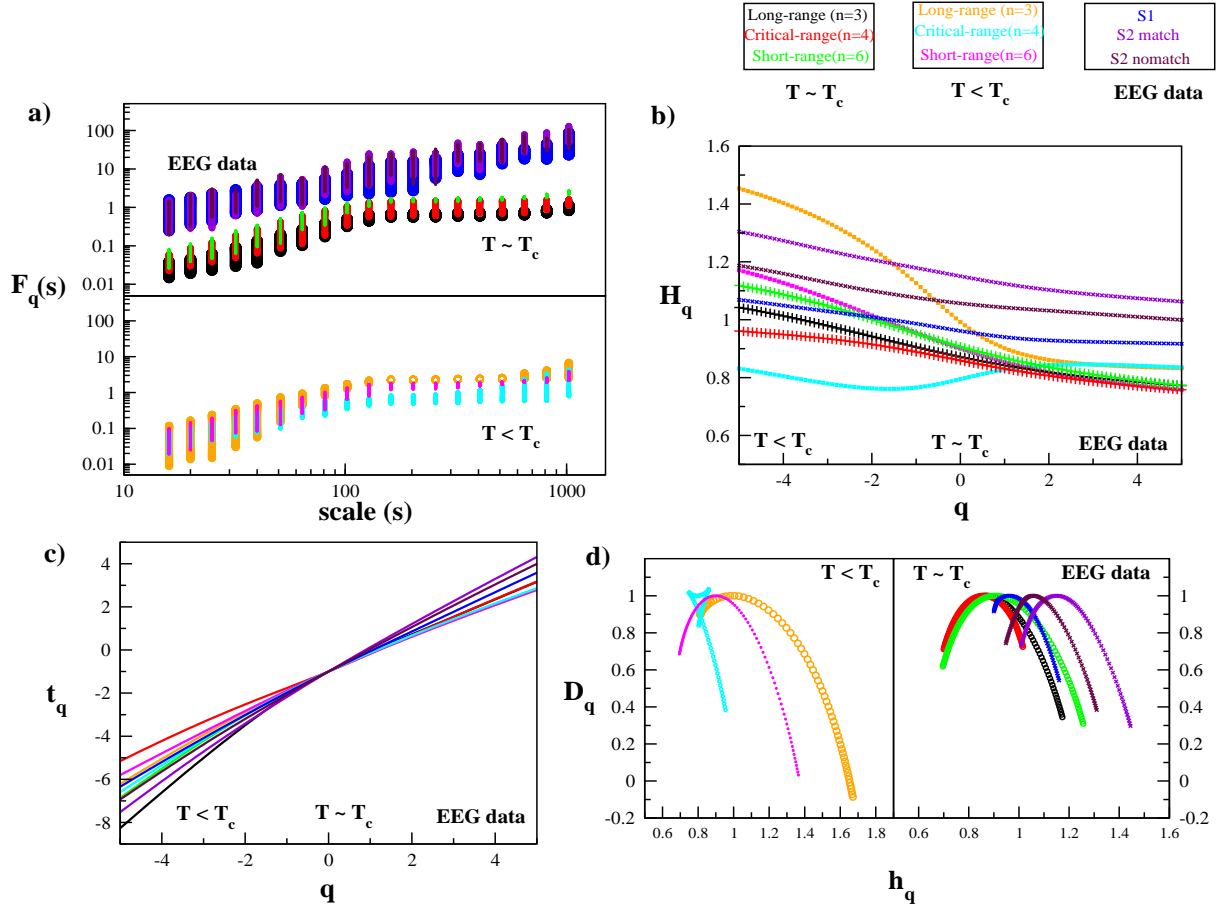


FIG. 6: **Multi-fractal detrended fluctuation analysis (MFDFA)** : The technique has been applied to the model-based FCPs at below and near-critical synaptic strengths and compared with the EEG-based FNs to determine multi-fractal nature. a) The q -order RMS fluctuation function F_q versus scale s , quantifies the scaling trend in fluctuations. b) The q -order Hurst exponent H_q , determines the scale of the fluctuation function F_q . c) The q -order singularity exponent t_q d) The q -order singularity exponent h_q versus Dimension D_q exhibits the multifractal spectrum. **Note-** The transition of FCPs at near-critical state is clear in the D_q versus h_q plot that exhibits a perfect arc of multifractal spectrum around the range of exponents and complements with the FNs of a visual task-based EEG data.

R7, kinless hubs (in Fig.4B), with inter-modular connections to broadcast the information. The FCPs of neurons exhibit the hierarchical and scale-free organization with distinct community/pattern formation, where, coordination of the hubs via cross-talking communities in the network is one of the key factors of information processing both at local and global levels of neuronal organization. In our study, it is evident that this mechanism of FCPs organization is rectified by local and global perturbations in it, which can be propagated throughout the network with the help of various ranges of interaction (short, critical and long-range interaction). This manifests the fractal properties of these FCPs, which further exhibited multifractal spectrum formation at near-critical strength. Thus, the near-critical transition state marks the onset of cognitive state through self organizing dynamics at near-criticality.

Brain dynamics is known to function at near-criticality. There are recent studies that depicts the non-linearity of the functional brain dynamics at the near-critical regime [18, 26, 64]. Our results of network theory attributes, fractal analysis and functional cartography have confirmed the generation of a scale-free hierarchical network (FCPs) only at the near-critical phase transition. We have made the following insights focussing on the basis of generation of these FCPs. The dynamics of these FCP's could procreate diverse cognitive states in the brain. These cognitive states could be thought of as a bunch of meta-stable states in a system with near dynamic equilibrium. The near-critical regime could accommodate a set of dynamic functional states whose synchronous permutational amalgamation could lead its way to cognitive behaviours. Also, from our study of near-critical dynamics for long, critical and short-ranged functional patterns, we have interpreted that criticality is a range and not just a point. As

Degree exponents:		α	β	γ	δ	ϵ	λ	κ
FCPs ($T \langle T_c \rangle$)	Long	-0.32	-0.03	0.1	0.1	1.04	1.99	-0.15
	Critical	-0.15	-0.01	0.42	0.2	0.99	1.98	-0.08
	Short	-0.34	-0.07	0.14	0.26	0.96	2.0	-0.10
FCPs ($T \simeq T_c$)	Long	-0.58	-0.34	-1.04	0.0	0.98	2.16	-1.11
	Critical	-0.4	-0.07	-0.6	0.08	0.88	1.97	-0.72
	Short	-0.35	0.0	-0.6	0.01	0.98	1.93	-0.78
EEG FNs	S1	-0.8	0.21	-2.31	0.10	1.6	2.92	-0.7
	S2 match	-0.73	0.23	-2.1	0.10	1.8	2.34	-0.78
	S2 nomatch	-0.73	0.21	-2.1	0.11	1.56	2.15	-0.87

TABLE I: The measure of degree exponents for various network theory attributes (as mentioned in section 4.3).

we found that the long-ranged dynamics require high coupling strength to attain criticality than the short-ranged. This explains how the increase in synaptic strength due to multiple stimulus attempts would make more long-range connections to the complex functional pattern in the brain. The dynamicity of long-range connections defines the task-specific functional connectivity at the global level [53]. Also, such analytical modelling of functional networks of neurons based on inter-neuronal coupling range could further assist in the extensive assessment of brain disorders, characterized by aberrant functional connectivity. The research in [30] have analyzed 2D Ising model to exhibit topological characterization of functional networks of neuronal activity at criticality, being more robust against structural defects. However, in brain disorders, such as ASD irregularity in the structural connectivity has caused less intricate long-ranged and denser short-ranged functional connectivity [21]. Also, the extent in reflection of structural connectivity changes on the topology of functional network cannot be determined till date and sounds debatable. Though, the research in [30] makes our belief more strong towards the critical phase transition state as the emerging functional state in the brain. We believe that our approach towards understanding the generation and characterization of functional patterns of neuronal activity in the brain cortex embarks us with new understanding on brain functional irregularities and also motivates modelling of functional connectivity in brain disorders.

There are obvious limitations that our model dynamics is binary and exhibits only firing/non-firing states of a neuron or group of neurons at a single lattice site. It overlooks the biochemical fluxes of a nerve cell and rather focuses on the global connectivity state. In our study, we have considered 64×64 lattice system for our model and the empirical data is from 64 electrodes over the brain, this surely sounds a huge gap. However, brain activity is known to follow statistical fractal nature, which allows the characteristic properties to remain similar over the size [29]. Also, we have addressed analytically that with an increase in system size the critical temperature will increase in the long-range regime, but this would not affect its near-critical dynamics. In spite of the huge complexity gap, we have got significant congruency in terms of the characteristic power law trends of the network topology between the task-specific functional brain networks and the FCPs at the near-critical regime only. This research has given us strong implication that the functional neuronal system supports far-from-equilibrium dynamics upon receiving a stimulus that leads to a second-order phase transition and self-organization is the key event that generates functional patterns in the brain cortex. This work gives us very useful insights towards the mechanistic view of the emerging brain functional connectivity, though there is still much more to dig and modelling through such simplistic model aid in understanding the concepts from a coarse lens that surely can be investigated to microscopic levels.

IV. METHODOLOGY

A. Network Construction:

The functional connectivity of neuronal population in the brain could be examined through a binary connectivity matrix where '1' represents the connection between two nodes and '0' is antithesis of '1' [59]. We have computed the functional connectivity based on statistical consanguinity of neuronal time-series using Pearson-correlation coefficient, used to measure inter-neuronal correlations [59]. The Pearson correlation coefficient r_{xy} , defines correlation between nodes x and y using the formula,

$$r_{xy} = \frac{\sum (x_i - \bar{x})(y_i - \bar{y})}{\sqrt{\sum (x_i - \bar{x})^2} \sqrt{\sum (y_i - \bar{y})^2}} \quad (8)$$

Where, x_i and y_i represents temporal data of two spins x and y for the total number of monte carlo steps. The binary undirected matrix is transformed into graph $G(S, E)$ consists of nodes set $S = \{s_i \mid i \in 1, \dots, N\}$ where N is the total spin sites i.e. 4096 in our study. Then, based on the functional correlation of spins the delineated edge list is defined as $E = \{e_{ij} \mid (s_i, s_j) \in S \times S\}$. We generated the binary connectivity matrix by averaging the data of 10 time-series from our model for each coupling range and global synaptic strength (Temperature). We applied a common thresholding limit for defining connections among the spins (neurons). We calculated the average correlation value in each case and then did the final average to get a unique threshold i.e. 0.2 for our model. This adjacency matrix is used to construct undirected networks for long, short and critical coupling range (n) at different overall synaptic strengths (T) employing NetworkX module in python. As we are studying the emergent behavior of our model generated functional patterns, we also constructed the functional brain cortical networks using the visibility graph approach on the EEG time-series data.

B. Visibility graph approach:

The EEG data has been taken from the UCI database, where the subjects were shown to three types of visual stimulus S1 (single image shown), S2_match (two similar images) and S2_nomatch (two dissimilar images) and recording was done using 64 electrodes with the sampling frequency of 256Hz for 1 second in healthy human subjects [5]. We applied the visibility graph approach in the EEG time-series data to construct the functional brain networks (FNs) generated while doing the visual task [41]. We took 10 trials for each type of stimulus. In this approach, each time state or neuronal state in the EEG time-series (or neuron activity pattern model based time-series) data, which is the resultant signal of the interacting neurons in the brain at that time state, is taken as node in the constructed network. The connections between any two time or neuronal states with data value n_a and n_b at time point t_a and t_b respectively would be defined if the third time step $n_c(t_c)$ satisfies the following condition,

$$\frac{n_b - n_c}{t_b - t_c} > \frac{n_b - n_a}{t_b - t_a} \quad (9)$$

The extracted network would be connected, at least to its neighbors, undirected and invariant according to the algorithm. The characteristic properties of the time-series get delineated in the form of resultant network.

C. Network theory attributes:

Network theory is the much applied theoretical approach by researchers for characterizing and studying complex brain networks [58]. We are providing some important attributes, which are used for our analysis, as given below.

Degree distribution

The probability of degree distribution to have degree k in a network defined by $G(N, E)$, where N and E are sets of nodes and edges of the network, is given by, $P(k) = \frac{n_k}{N}$, where, n_k and N are number of nodes having k degree and size of the network, respectively [47]. The degree distribution, $P(k)$, for the Erdős-Reányi random network follows Poisson distribution and deviates from the random for small-world networks, whereas, for scale-free and hierarchical networks it follows power-law, $P(k) \sim k^{-\gamma}$, where, $2 < \gamma < 3$ [1, 2].

Clustering co-efficient

Clustering co-efficient, which characterizes how strongly a node is connected to the rest of the nodes in the network, of an i th node in the network, can be estimated as the ratio of the number of its nearest neighborhood edges to the total possible number of edges of degree k_i , $C(k_i) = \frac{E_i}{k_i C_2}$, where, E_i and k_i are the number of connected pairs of nearest-neighbors of i th node [47]. $C(k) \rightarrow \text{constant}$ for scale-free, random and small-world networks, whereas, for hierarchical network, $C(k) \sim k^{-\alpha}$, with $\alpha \sim 1$ [1, 2].

Neighborhood connectivity

It is characterized by the measure of mean connectivities of the nearest neighbors of each node in a network given by, $C_n(k) = \sum_u u P(u|k)$, where, $P(u|k)$ is the probability that a link belongs to a node with degree k points to a node with connectivity u [44, 54]. The hierarchical network follows, $C_n(k) \sim k^{-\beta}$, with $\beta \sim 0.5$ [54]. However, if $C_n(k) \sim k^\beta$ (positive β), then the network exhibits assortative nature indicating the possibility of coordinating high

degree hubs in the network.

Betweenness centrality

Betweenness centrality of a node w is the measure of sharing amount that a node i needs w to reach j via shortest path, and is given by, $C_B(w) = \sum_{i,j;i \neq j \neq w} \frac{d_{ij}(w)}{d_{ij}}$, where, $d_{ij}(w)$ is the number of geodesic paths from node i to j passing through w , and d_{ij} indicates number of geodesic paths from node i to j [42]. It characterizes the amount of information traffic diffusing from each node to every other node in the network [11].

Closeness centrality

Closeness centrality of a node u is characterized by the harmonic mean of the geodesic paths connecting u and any other nodes in the network, $C_C(u) = \frac{n}{\sum_i d_{ui}}$, where, d_{ui} is the geodesic path length between nodes u and i , and n is total number of nodes connected to node u in the network [15]. It generally measures the rate of information flow in the network, where, larger the value of C_C corresponds short path lengths, and hence fast information processing in the network, and vice versa [11].

Eigen-vector centrality

Eigen-vector centrality of a node w in a network, which indicates the power of spreading of a particular node in the network, can be expressed by, $C_E(w) = \frac{1}{\lambda} \sum_{i \in nn(w)} u_i$, where, $nn(w)$ is the nearest neighbors of node w , λ is the eigenvalue of eigenvector v_i $Av_i = \lambda v_i$, A is the adjacency matrix of the network [15]. The principal eigenvector of A , which satisfy $Au_w = \lambda_{max}$, is taken to have positive eigenvector centrality score.

Rich-club co-efficient

Rich nodes correspond to nodes having large links in the network, and they tend to form tight subgraph among them, which is referred to as rich-club formation in the network [68]. This rich-club phenomenon can be quantified by rich-club coefficient defined by, $R_C(k) = \frac{E_{>k}}{N_{>k} C_2}$, where, $E_{>k}$ as the number of edges after removing nodes less than degree k distributed among $N_{>k}$ nodes [20]. It characterizes many important properties of the network, namely, information traffic backbone, mixing properties of the network, etc. The rich-club organization analysis has been done to estimate the presence of connector hubs. The Brain connectivity toolbox has been used to compute the rich-club coefficient and network centrality measures [56, 59].

Participation index

The participation coefficient (P_i) signifies the distribution of connections of a particular node i with respect to different communities [32] given by,

$$P_i = 1 - \sum_{c=1}^N \left(\frac{k_{ic}}{k_i} \right)^2, \quad (10)$$

where, k_{ic} is the number of connections made by node i to nodes in module c and k_i is the total degree of node i . The P_i value determines the distributional uniformity of the neuronal connections, specified by the range 0-1. The escalating value signifies a more homogeneous allocation of links among all the modules.

The **within-module degree** Z_i is another measure to quantify the role of a particular node i in the module c_i . High values of Z_i indicate more intra-community connections than inter-community and vice-versa [32].

$$Z_i = \frac{k_i - \bar{k}_{c_i}}{\sigma_{k_{c_i}}}, \quad (11)$$

where, k_i is the number of connections of the node i to other nodes in its module c_i . \bar{k}_{c_i} is the average k over all nodes in the module c_i and $\sigma_{k_{c_i}}$ is the standard deviation of k in c_i .

Community detection method:

The complex network structure can be forbidden into communities or modules, specified with less than expected number of connections among them. We have used the community Louvain method to design non-overlapping communities out of the network [9]. This method has outperformed other methods in terms of both modularity and computational time [9]. To create a significant division of a network the benefit function called modularity (Q) is defined as,

$$Q = \frac{1}{W} \sum_{i,j=1}^N [A_{ij} - B_{ij}] \delta_{c_i, c_j}, \quad (12)$$

The modularity Q , is maximized for good partitioning of the graph $G(S, E)$ with N as total nodes. The A_{ij} and B_{ij}

defines the exact and expected number of connections between nodes i and j . $W = \sum_{i,j} A_{ij}$, c_i and c_j are the communities nodes i and j belongs to, δ_{c_i, c_j} equals to 1, when nodes i and j falls in same community and 0, if they do not.

D. MFDFA analysis:

Multi-fractal detrended fluctuation analysis (MFDFA) approach has been used to ensure the fractality of dynamic patterns generated over non-stationary temporal data in complex biological systems [25, 37]. The statistical fractals generated through physiological time-series data show self affinity in terms of different scaling with respect to direction [25]. The presence of multiple scaling exponents can be examined in a time-series using the Matlab formulation of the MF-DFA method [36]. Parameters characterizing multifractality are scaling function (F), Hurst exponent (H), mass exponent (t), singularity exponent (h) and Dimension (D) as explained in [36]. For a time-series signal x_j of finite length l with random walk like structure, can be computed by the Root mean square (RMS) variation, $X_i = \sum_{j=1}^i (x_j - \langle x \rangle)$, where, $\langle x \rangle$ is the mean value of the signal, and $i = 1, 2, \dots, l$. The signal X has been divided into $n_s = \text{int}(\frac{l}{s})$ non-overlapping segments of equal size s . To avoid left-over short segments at the end, the counting has been done from both sides therefore $2n_s$ segments are taken into account. This defines the scale (s) to estimate the local fluctuations in the time-series. Thus, the overall RMS, F , for multiple scales can be computed using the equation,

$$F^2(s, v) = \frac{1}{s} \sum_{i=1}^s \{X[(v-1)s + i] - x_v(i)\}^2 \quad (13)$$

where, $v = 1, 2, \dots, n_s$ and $x_v(i)$ is the fitting trend in each segment v . The q -order RMS fluctuation function further determines the impact of scale (s) with large (+ q 's) and small (- q 's) fluctuations, as follows,

$$F_q(s) = \left\{ \frac{1}{2n_s} \sum_{\nu=1}^{2n_s} [F^2(\nu, s)]^{\frac{q}{2}} \right\}^{\frac{1}{q}} \quad (14)$$

The q -dependent fluctuation function $F_q(s)$ for each scale (s) will quantify the scaling behaviour of the fluctuation function for each q ,

$$F_q(s) \sim s^{H_q} \quad (15)$$

where, H_q is the generalized Hurst exponent, one of the parameters that characterize multi-fractality through small and large fluctuations (negative and positive q 's) in the time-series. The H_q is related to q -order mass exponent t_q as follows,

$$t_q = qH_q - 1 \quad (16)$$

from t_q , the singularity exponent h_q and Dimension D_q is defined as,

$$h_q = \frac{dt_q}{dq}, \quad D_q = qh_q - t_q \quad (17)$$

The plot of D_q versus h_q represents the multifractal spectrum of the time-series.

V. CONFLICT OF INTEREST STATEMENT

The authors declare no competing financial interests.

VI. AUTHOR CONTRIBUTIONS

R.K.B.S. and J.G. conceived the model. J.G. did the numerical experiment and prepared the figures of the numerical results. J.G. and R.K.B.S. analyzed and interpreted the results, and wrote the manuscript. All author read and approved the manuscript.

VII. FUNDING

J.G. and R.K.B.S. are financially supported by Council of Scientific and Industrial Research through sanctioned project 25(0221)/13/EMR-II.

VIII. ACKNOWLEDGMENTS

We acknowledge the funding agencies and Jawaharlal Nehru University. This manuscript has been released as a Pre-Print at [<https://www.biorxiv.org/content/10.1101/569244v1>] [34].

IX. DATA AVAILABILITY STATEMENT

The dataset analyzed for this study can be found in the [UCI machine learning repository: EEG database data set [<https://archive.ics.uci.edu/ml/datasets/EEG+Database>]].

-
- [1] Albert, R. and Barabási, A.-L. (2002). Statistical mechanics of complex networks. *Reviews of modern physics*, 74(1):47.
 - [2] Barabasi, A.-L. and Oltvai, Z. N. (2004). Network biology: understanding the cell's functional organization. *Nature reviews genetics*, 5(2):101.
 - [3] Bassett, D. S., and Gazzaniga, M. S. (2011). Understanding complexity in the human brain. *Trends in cognitive sciences*, 15(5):200–209.
 - [4] Beggs, J. M. and Plenz, D. (2003). Neuronal Avalanches in Neocortical Circuits. *The Journal of Neuroscience*, 23(35):11167–11177.
 - [5] Beggs, J. M. and Timme, N. (2012). Being Critical of Criticality in the Brain. *Frontiers in Physiology*, 3(June):1–14.
 - [6] Begleiter, H. (1999). UCI machine learning repository: EEG database data set.
 - [7] Binder, K. and Heermann, D. W. (1988). *Monte Carlo Simulation in Statistical Physics*. Springer Berlin Heidelberg.
 - [8] Blanchard, T., Picco, M., and Rajabpour, M. a. (2013). Influence of long-range interactions on the critical behavior of the Ising model. *EPL (Europhysics Letters)*, 101(5):56003.
 - [9] Blondel, V., Guillaume, J.-L., Lambiotte, R., and Lefebvre, E. (2008). Fast unfolding of communities in large networks. *Journal of Statistical Mechanics: Theory and Experiment*, 2008(10):P10008.
 - [10] Bonacich, P. (1972). Factoring and weighting approaches to status scores and clique identification. *Journal of mathematical sociology*, 2(1):113–120.
 - [11] Borgatti, S. P. (2005). Centrality and network flow. *Social networks*, 27(1):55–71.
 - [12] Bruijn, N. d. (1981). *Asymptotic methods in analysis*. Dover Publications, Inc. New York.
 - [13] Bullmore, E. and Sporns, O. (2009). Complex brain networks: graph theoretical analysis of structural and functional systems. *Nature reviews. Neuroscience*, 10(3):186–198.
 - [14] Cannas, S. A. and Tamarit, F. A. (1996). Long-range interactions and nonextensivity in ferromagnetic spin models. *Physical Review B*, 54(18):R12661–R12664.
 - [15] Canright, G. and Engö-Monsen, K. (2004). Roles in networks. *Science of Computer Programming*, 53(2 SPEC. ISS.):195–214.
 - [16] Chialvo, D. R. (2010). Emergent complex neural dynamics. *Nature Physics*, 6(10):744–750.
 - [17] Clauset, A., Shalizi, C. R., and Newman, M. E. (2009). Power-law distributions in empirical data. *SIAM review*, 51(4):661–703.
 - [18] Cocchi, L., Gollo, L. L., Zalesky, A., and Breakspear, M. (2017). Criticality in the Brain: A synthesis of neurobiology, models and cognition. *Progress in neurobiology*, 158:132–152.
 - [19] Colicos, M. a. and Syed, N. I. (2006). Neuronal networks and synaptic plasticity: understanding complex system dynamics by interfacing neurons with silicon technologies. *The Journal of experimental biology*, 209(Pt 12):2312–2319.
 - [20] Colizza, V., Flammini, A., Serrano, M. A., and Vespignani, A. (2006). Detecting rich-club ordering in complex networks. *Nature*, 2(February):110–115.

- [21] Conti, E., Mitra, J., Calderoni, S., Pannek, K., Shen, K. K., Pagnozzi, A., Rose, S., Mazzotti, S., Scelfo, D., Tosetti, M., Muratori, F., Cioni, G., and Guzzetta, A. (2017). Network over-connectivity differentiates autism spectrum disorder from other developmental disorders in toddlers: A diffusion MRI study. *Human Brain Mapping*, 38(5):2333–2344.
- [22] De Domenico, M., Sasai, S., and Arenas, A. (2016). Mapping multiplex hubs in human functional brain networks. *Frontiers in Neuroscience*, 10(JUL):1–14.
- [23] Deco, G., Senden, M., and Jirsa, V. (2012). How anatomy shapes dynamics: a semi-analytical study of the brain at rest by a simple spin model. *Frontiers in Computational Neuroscience*, 6(September):1–7.
- [24] Eguíluz, V. M., Chialvo, D. R., Cecchi, G. A., Baliki, M., and Apkarian, A. V. (2005). Scale-free brain functional networks. *Physical Review Letters*, 94(1):1–4.
- [25] Eke, a., Herman, P., Kocsis, L., and Kozak, L. R. (2002). Fractal characterization of complexity in temporal physiological signals. *Physiological measurement*, 23(1):R1–R38.
- [26] Ezaki, T., dos Reis, E. F., Watanabe, T., Sakaki, M., and Masuda, N. (2020). Closer to critical resting-state neural dynamics in individuals with higher fluid intelligence. *Communications Biology*, 3(1):1–9.
- [27] Fisher, M. E., Ma, S.-k., and Nickel, B. G. (1972). Critical Exponents for Long-Range Interactions. *Physical Review Letters*, 29(14):917–920.
- [28] Fraiman, D., Balenzuela, P., Foss, J., and Chialvo, D. R. (2009). Ising-like dynamics in large-scale functional brain networks. *Phys. Rev. E*, 79(6):61922.
- [29] Franca, L. G. S., Miranda, J. G. V., Leite, M., Sharma, N. K., Walker, M. C., Lemieux, L., and Wang, Y. (2018). Fractal and multifractal properties of electrographic recordings of human brain activity: toward its use as a signal feature for machine learning in clinical applications. *Frontiers in physiology*, 9:1767.
- [30] Goodarzinick, A., Nir, M. D., Valizadeh, A., and Perc, M. (2018). Robustness of functional networks at criticality against structural defects. *Physical Review E*, 98(2):022312.
- [31] Grüneberg, D. and Hucht, A. (2004). Universal finite-size scaling analysis of Ising models with long-range interactions at the upper critical dimensionality: Isotropic case. *Physical Review E*, 69(3):036104.
- [32] Guimerà, R. and Amaral, L. (2005). Functional cartography of complex metabolic networks. *Nature*, 433:895–900.
- [33] Gundh, J., Singh, A., and Singh, R. K. B. (2015). Ordering Dynamics in Neuron Activity Pattern Model: An Insight to Brain Functionality. *PLoS ONE*, 10(1932-6203 (Electronic)):e0141463.
- [34] Gund, J. and Singh, R. K. B. (2019). Emergence of Functional Cortical Patterns of neurons characterize the self-organizing way to cognition in brain. <https://www.biorxiv.org/content/10.1101/569244v1>
- [35] Hiley, B. J. and Joyce, G. S. (1965). The Ising model with long-range interactions. *Proceedings of the Physical Society*, 85(3):493.
- [36] Ihlen, E. A. F. (2012). Introduction to multifractal detrended fluctuation analysis in Matlab. *Frontiers in Physiology*, 3 JUN(June):1–18.
- [37] Kantelhardt, J. W., Zschiegner, S. A., Koscielny-Bunde, E., Havlin, S., Bunde, A., and Stanley, H. E. (2002). Multifractal detrended fluctuation analysis of nonstationary time series. *Physica A*, 316(1-4):87–114.
- [38] Kauffman, S. A. (1993). The origins of order: Self-organization and selection in evolution. OUP USA.
- [39] Kitzbichler, M. G., Smith, M. L., Christensen, S. R., and Bullmore, E. (2009). Broadband Criticality of Human Brain Network Synchronization. *PLoS Computational Biology*, 5(3):e1000314.
- [40] Klinshov, V. V., Teramae, J.-n., Nekorkin, V. I., and Fukai, T. (2014). Dense Neuron Clustering Explains Connectivity Statistics in Cortical Microcircuits. *PLoS ONE*, 9(4):e94292.
- [41] Lacasa, L., Luque, B., Ballesteros, F., Luque, J., and Nuno, J. C. (2008). From time-series to complex networks: The visibility graph. *Proceedings of the National Academy of Sciences*, 105(13):4972–4975.
- [42] Linton C. Freeman (1978). Centrality in Social Networks Conceptual Clarification. *Social Networks*, 179(1968):215–239.
- [43] Luria, A. R. (1980). *Higher cortical functions in man*. Basic Books.
- [44] Maslov, S. and Sneppen, K. (2002). Specificity and stability in topology of protein networks. *Science*, 296(5569):910–913.
- [45] McCoy, B. M., and Wu, T. T. (2014). *The two-dimensional Ising model*. Dover publications: New York, USA.
- [46] Meunier, D., Lambiotte, R., and Bullmore, E. T. (2010). Modular and hierarchically modular organization of brain networks. *Frontiers in Neuroscience*, 4(DEC):1–11.
- [47] Newman, M. (2009). *Networks: An Introduction*. OUP Oxford.
- [48] Newman, M. and Barkema, G. (1999). *Monte carlo methods in statistical physics chapter 1-4*. Oxford University Press: New York, USA.
- [49] Newman, M. E. J. (2006). Modularity and community structure in networks. *Proceedings of the National Academy of Sciences of the United States of America*, 103(23):8577–8582.
- [50] Nigam, S., Shimono, M., Ito, S., Yeh, F.-C., Timme, N., Myroshnychenko, M., Lapsch, C. C., Tosi, Z., Hottowy, P., Smith, W. C., Masmanidis, S. C., Litke, A. M., Sporns, O., and Beggs, J. M. (2016). Rich-Club Organization in Effective Connectivity among Cortical Neurons. *Journal of Neuroscience*, 36(3):670–684.
- [51] Onsager, L. (1944). Crystal statistics. i. a two-dimensional model with an order-disorder transition. *Physical Review*, 65(3-4):117.
- [52] Papo, D., Buldu, J. M., Boccaletti, S., and Bullmore, E. T. (2014). Complex network theory and the brain. *Philosophical Transactions of the Royal Society B: Biological Sciences*, 369(1653):20130520–20130520.
- [53] Park, H. J., and Friston, K. (2013). Structural and Functional Brain Networks: From Connections to Cognition. *Science*, 342(6158):1238411–1238411.
- [54] Pastor-Satorras, R., Vázquez, A., and Vespignani, A. (2001). Dynamical and correlation properties of the internet. *Physical review letters*, 87(25):258701.

- [55] Picco, M. (2012). Critical behavior of the Ising model with long-range interactions. *arXiv preprint arXiv:1207.1018*.
- [56] Rubinov, M. and Sporns, O. (2010). Complex network measures of brain connectivity: Uses and interpretations. *NeuroImage*, 52(3):1059–1069.
- [57] Song, S., Sjöström, P. J., Reigl, M., Nelson, S., and Chklovskii, D. B. (2005). Highly nonrandom features of synaptic connectivity in local cortical circuits. *PLoS biology*, 3(3):e68.
- [58] Sporns, O. (2002). Network analysis, complexity, and brain function. *Complexity*, 8(1):56–60.
- [59] Sporns, O. (2007). Brain connectivity. *Scholarpedia*, 2(10):4695.
- [60] Sporns, O., Chialvo, D. R., Kaiser, M., and Hilgetag, C. C. (2004). Organization, development and function of complex brain networks. *Trends in Cognitive Sciences*, 8(9):418–425.
- [61] Sporns, O., Tononi, G., and Edelman, G. M. (2000). Theoretical Neuroanatomy: Relating Anatomical and Functional Connectivity in Graphs and Cortical Connection Matrices. *Cerebral Cortex*, 10(2):127–141.
- [62] Sporns, O., Tononi, G., and Edelman, G. M. (2002). Theoretical neuroanatomy and the connectivity of the cerebral cortex. *Behavioural Brain Research*, 135(1-2):69–74.
- [63] Stam, C. J., Jones, B. F., Nolte, G., Breakspear, M., and Scheltens, P. (2007). Small-world networks and functional connectivity in Alzheimer’s disease. *Cerebral Cortex*, 17(1):92–99.
- [64] Tagliazucchi, E., Chialvo, D. R., Siniatchkin, M., Amico, E., Brichant, J. F., Bonhomme, V., and Laureys, S. (2016). Large-scale signatures of unconsciousness are consistent with a departure from critical dynamics. *Journal of The Royal Society Interface*, 13(114):20151027.
- [65] Teller, S., Granell, C., De Domenico, M., Soriano, J., Gómez, S., and Arenas, A. (2014). Emergence of assortative mixing between clusters of cultured neurons. *PLoS computational biology*, 10(9):e1003796.
- [66] Thomas Yeo, B. T., Krienen, F. M., Eickhoff, S. B., Yaakub, S. N., Fox, P. T., Buckner, R. L., Asplund, C. L., and Chee, M. W. L. (2015). Functional specialization and flexibility in human association cortex. *Cerebral Cortex*, 25(10):3654–3672.
- [67] Voglis, G. and Tavernarakis, N. (2006). The role of synaptic ion channels in synaptic plasticity. *EMBO reports*, 7(11):1104–10.
- [68] Zhou, S. and Mondragón, R. J. (2004). The rich-club phenomenon in the internet topology. *IEEE Communications Letters*, 8(3):180–182.